One-dimensional lead-free perovskite single crystal with high X-ray response grown by liquid phase diffusion

Chang-Feng Wang,† Cui-Ling Fang,† Yan Feng, Shi-Yu Liu, Yi Zhang, Heng-Yun Ye, Le-Ping Miao and Lang Liu*

1. Experimental section

1.1 Synthesis methods

1.1.1 Temperature cooling method

A mixture of 1,5-pentanediamine iodide (2 mmol, 0.712 g) and BiI_3 (2 mmol, 1.18 g) in aqueous HI solution (55.0% - 58.0%, about 30 mL) was heated and stirred at 405 K until a clear solution was formed. The solution was allowed to cool at a rate of 2 K h^{-1}, which yielded black crystals.

1.1.2 Liquid phase diffusion method

First, an H-shaped test tube was placed somewhere undisturbed. 1,5-pentanediamine iodide (5 mmol, 1.78 g) and BiI_3 (5 mmol, 2.95 g) were dissolved in aqueous HI solution (55.0% - 58.0%, about 25 mL), respectively. These solutions were completely stirred at room temperature for 3 h and then filtered to obtain transparent precursor solutions. Then, 1,5-pentanediamine iodide and BiI_3 precursor solutions were transferred into test tubes A and C, respectively, as shown in Figure 2a. Finally, aqueous HI solution (55.0% - 58.0%, about 20 mL) was carefully added to the test tube in drops along the wall. Glass stoppers seal the orifice to prevent the HI from oxidizing. After a month, black crystals were obtained in test tube B.

1.2 Determination of single crystal structure

Single dull dark black plank-shaped crystals of (1,5-PDA)BiI_5 were used as supplied. A suitable crystal with dimensions 0.35 × 0.22 × 0.21 mm^3 was selected and mounted on a XtaLAB Synergy R, HyPix diffractometer. The crystal was kept at a steady T = 302 K during data collection. The structure was solved with the ShelXT 2014/5 (Sheldrick, 2014) solution program using iterative methods and by using Olex2 1.5-alpha (Dolomanov et al., 2009) as the graphical interface.[1-2] The model was refined with ShelXL 2018/1 (Sheldrick, 2015) using full matrix least squares minimization on F^2.[3]

he X-ray crystallographic structures have been deposited at the Cambridge Crystallographic Data Centre (deposition numbers 2207566), and can be obtained free of charge from the CCDC via www.ccdc.cam.ac.uk/ get structures.

References:

1. O.V. Dolomanov and L.J. Bourhis and R.J. Gildea and J.A.K. Howard and H. Puschmann, Olex2: A complete structure solution, refinement and analysis program, *J. Appl. Cryst.*, (2009), **42**, 339-341.

2. Sheldrick, G.M., ShelXT-Integrated space-group and crystal-structure determination, *Acta Cryst.*, (2015), **A71**, 3-8.

3. Sheldrick, G.M., Crystal structure refinement with ShelXL, *Acta Cryst.*, (2015), **C71**, 3-8.

1.3 Evaluation of distortion of octahedra

The calculation of Δd.

$$\Delta d = \left(\frac{1}{6}\right)\sum (d_i - d_0)^2/{d_0}^2 = 0.03909$$

Where Δd is distortion index; d_i is Bi–I bond length; d_0 is the average Bi–I bond length.

The calculation of σ^2.

$$\sigma^2 = \sum_{i=1}^{12} \frac{(\theta_i - 90)^2}{11} = 18.55\ {}^{\circ 2}$$

Where σ^2 is bond angle variance; θ_i is I–Bi–I bond angle.

1.4 Hirshfeld surfaces analysis

Hirshfeld surfaces and two-dimensional (2D) fingerprint plots were calculated by the CrystalExplorer software.[1] CIF format of (1,5-PDA)BiI_5 in room temperature was adopted for providing structural information. The calculation resolution is high (standard). Normalized contact distance (d_{norm}) is defined by equation 1, in which, d_i/d_e represents a distance from a point on the surface to the nearest nucleus outside/inside the surface; r_i^{vdW}/r_e^{vdW} is the van der Waals (vdW) radius of the appropriate atom internal/external to the surface.

$$d_{norm} = \frac{d_i - r_i^{vdW}}{r_i^{vdW}} + \frac{d_e - r_e^{vdW}}{r_e^{vdW}} \qquad (equation\ 1)$$

The negative/positive d_{norm} suggests contact shorter/greater than vdW separations. When d_{norm} is mapped on Hirshfeld surface, a red-white-blue color scheme is adopting for displaying d_{norm}, where red highlights shorter contacts, white is used for contacts around the vdW separation, and blue is for longer contacts. 2D fingerprint plots are created by binning (d_i, d_e) pairs in intervals of 0.01 A˚. Coloring each bin (essentially a pixel) of the resulting 2D histogram as a function of the fraction of surface points in that bin, ranging from blue (few points) through green to red (many points).

References:

[1] P. R. Spackman, M. J. Turner, J. J. McKinnon, S. K. Wolff, D. J. Grimwood, D. Jayatilaka, M. A. Spackman, *J. Appl. Crystallogr*. **2021**, *54*, 1006.

1.5 PXRD measurements

The Rigaku D/MAX 2000 x-ray diffractometer adopting Cu-Kα radiation (λ = 0.15406 nm, 40 kV and 40 mA) and a secondary beam graphite monochromator was used to perform PXRD measurement. Measurement angle ranges from 5° to 50° with step size of 0.02° and scanning speed 2° min^{-1}.

1.6. Thermogravimetric measurements

Thermogravimetric (TG) measurements were recorded on a NETZSCH TG 209F3 apparatus under an N_2 atmosphere with a heating rate of 10 K min^{-1}.

1.7 UV–vis diffuse reflectance spectroscopy measurements

Ultraviolet–visible (UV–vis) diffuse reflectance spectroscopy measurements were performed at 303 K using a Shimadzu (Tokyo, Japan) UV-2600 spectrophotometer with an ISR–2600 Plus integrating sphere operating from 200 to 800 nm. The powder crystals of (1,5-pentanediamine)BiI_5 were used for UV−vis absorption spectrum measurements. $BaSO_4$ was used as a 100% reflectance reference.

1.8 The fitting bandgap

The optical bandgap was determined from the fitting of the variant *Tauc* equation for direct bandgap:

$$((h\nu \bullet F(R_\infty))^2 = A(h\nu - E_g)$$

where h is Planck constant, ν is the frequency of the photon, $F(R_\infty)$ is the Kubelka−Munk function, and A is a proportional constant.

1.9 DFT calculation

First-principles DFT calculation was performed with single-crystal structure date of (1,5-PDA)BiI_5 by the Cambridge Sequential Total Energy Package (CASTEP). The exchange-correlation functional was described by a generalized gradient approximation (GGA) with Perdew−Burke−Ernzerhof (PBE) functional scheme. The interactions between the ionic cores and the electrons were described by the Ultrasoft pseudopotential. The following orbital electrons were treated as valence electrons: H, 1s1; C, 2s2 2p2; N, 2s2 2p3; F 2s2 2p5; Bi, 6s2 6p3; I 5s2 5p5. a Monkhorst - Pack k-point sampling of 2×1×1 and an energy cutoff adopted 517 eV.

1.10 Fabrication of planar (1,5-PDA) BiI_5 single-crystal detectors

The planar SC X-ray detector was fabricated by vacuum evaporation deposition of parallel Au electrodes (120 nm thickness) on the SC surface. Each device has an area of 0.15 mm^2.

1.11 Characterization of dielectric constant of (1,5-PDA)BiI_5 SCs

We used Au/(1,5-PDA)BiI_5/Au as the dielectric device, and the dielectric constant (ε = 27.8) was directly measured by Tonghui TH2828A analyzer. (1,5-PDA)BiI_5 is used as the dielectric layer, and its electrode area is 18.62 mm^2 and the crystal thickness is 1.45 mm.

1.12 Photoconductivity measurements

We use vertical structure to conduct photoconductivity measurements, wherein Au with a thickness of 120 nm was evaporated on both sides of the SC to form an Au/(1,5-PDA)BiI_5/Au structure with a device area of 18.42 mm^2 and a crystal thickness of 1.45 mm. A modified Hecht equation was used to fit the obtained result, deriving the information of μτ product and surface recombination velocity *s*.

$$I = \frac{I_0 \mu\tau V}{L^2} \frac{1 - exp(-\frac{L^2}{\mu\tau V})}{1 + \frac{Ls}{V\mu}}$$

where I_0 is the saturated photocurrent, L is the thickness, V is the applied bias, τ is the carrier lifetime. The fitting curve was shown in Figure 4c.

1.13 X-ray detector performance measurements

X-ray detection performance was measured on the measurement system in the DX-2700B X-ray diffractometer. All X-ray response characterizations were performed directly in a dark air environment to minimize electromagnetic and ambient light interference. A DS2901/24 X-ray tube with a tungsten target and 2.4kW output power was used as the source. Different radiation dose rates can be obtained by adjusting the values of accelerating voltage and working current. Aluminum sheets of different thicknesses were inserted between the X-ray source and the (1,5-PDA)BiI_5 detector as attenuators. The X-ray radiation dose rate was also calibrated using an Accu-Gold digitizer.

1.14 Characterization of (1,5-PDA)BiI_5 SCs mobility

When operating in Child's regime, I-V curve follows the Mott-Gurney law:

$$J_D = \frac{9}{8}\varepsilon\varepsilon_0\mu\frac{V^2}{L^3}$$

Where μ is the carrier mobility and V is the bias voltage, ε_0 is the vacuum permittivity, ε is the relative dielectric constant, L is the thickness of SCs. Thereby, we could estimate the carrier mobility in this region.

2. Supporting Figures

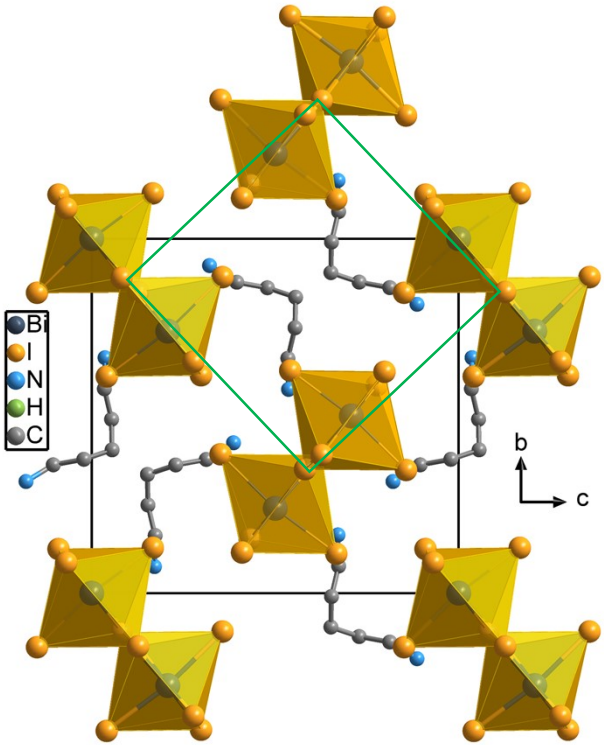

Fig. S1. The packing structure of (1,5-PDA)BiI_5 viewing along the *a*-axis direction. The green box represents cavities that can be seen as composed of the four $(BiI_5)_n^{2n-}$ zigzag chains.

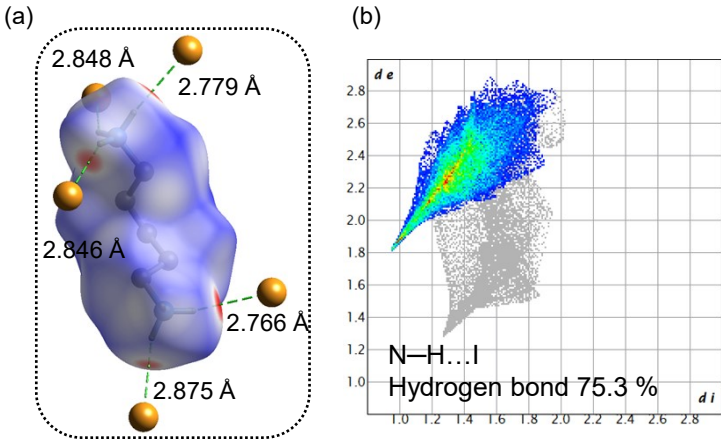

Fig. S2 (a) Hirshfeld surface mapped with d_{norm} and distribution of hydrogen bonds for 1,5-PDA

cation. (b) Fingerprint plots for 1,5-PDA cation resolved into N-H…I hydrogen bond.

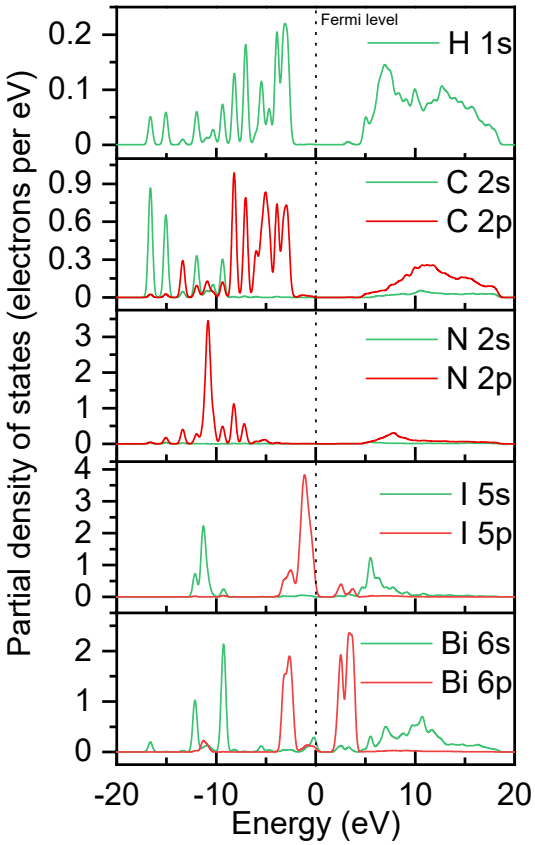

Fig. S3 PDOS of (1,5-PDA)BiI_5.

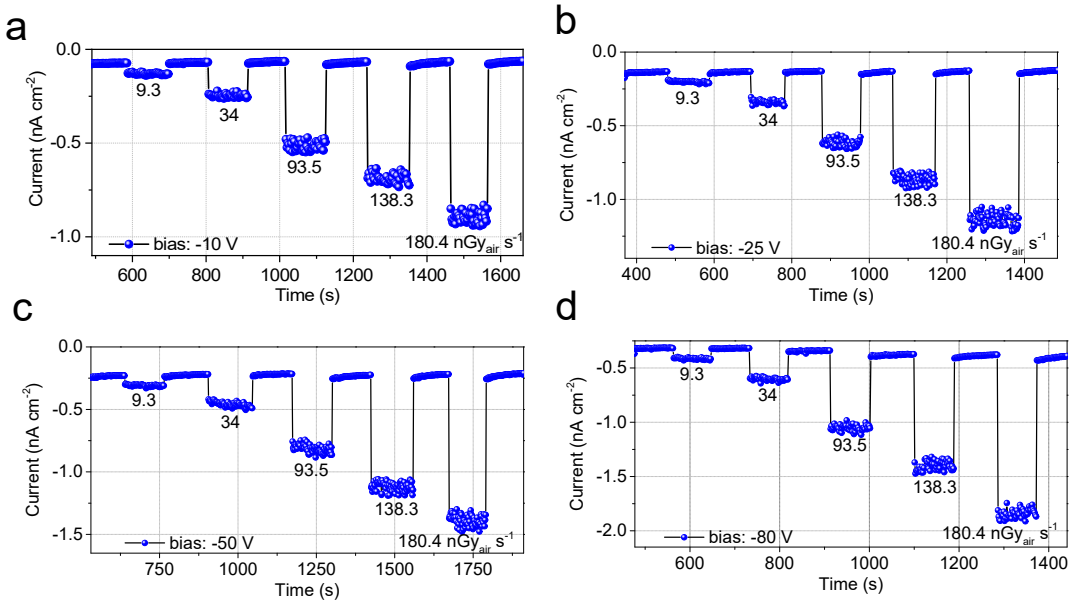

Fig. S4 Photoelectric response curve of the (1,5-PDA)BiI_5 detector under different doses and bias voltage: (a) -10 V, (b) -25 V, (c) -50 V, and (d) -80 V.

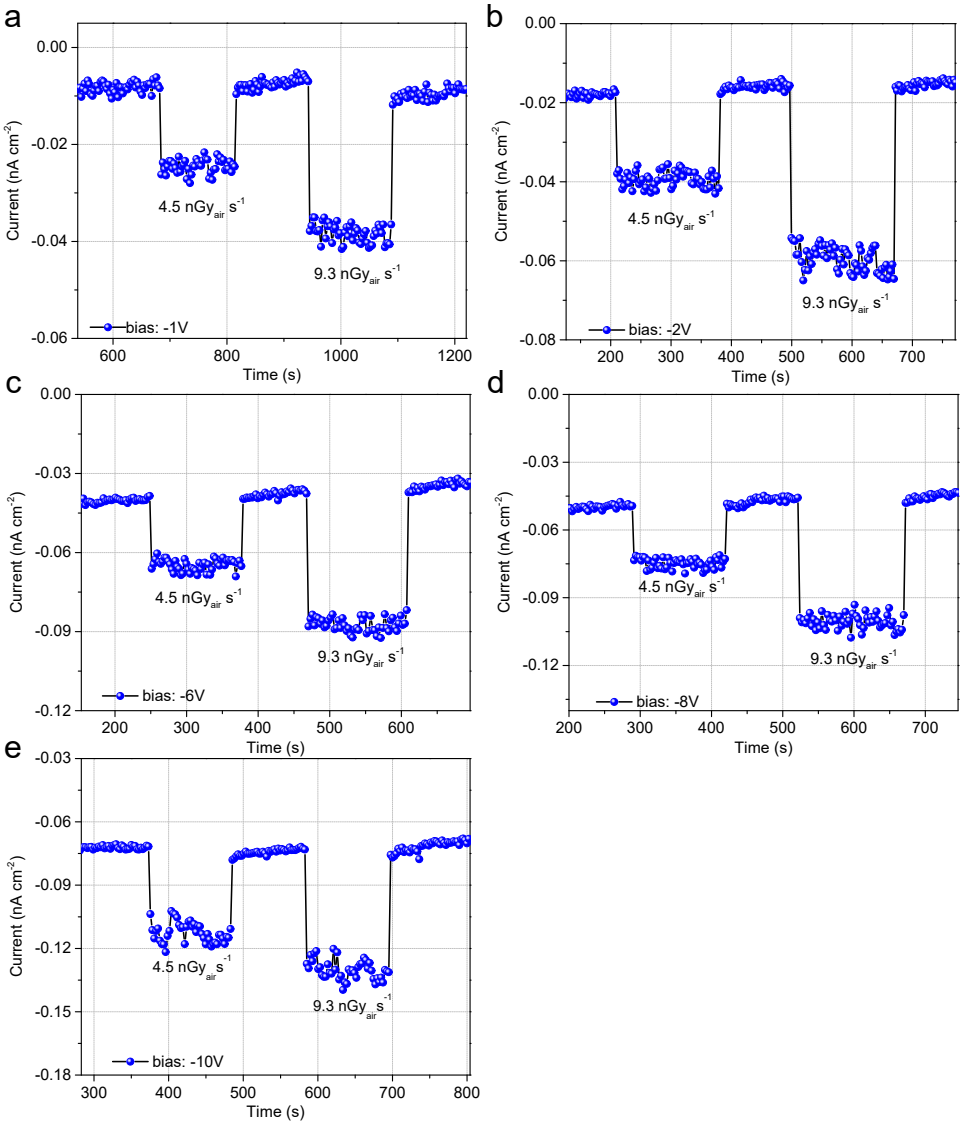

Fig. S5 Weak light response of the (1,5-PDA)BiI_5 detector under different bias voltages: (a) -1 V, (b) -2 V, (c) -6 V, (d) -8 V, and (e) -10 V.

3. Supporting Tables

Table S1. Crystal data for (1,5-PDA)BiI5 at 302.15 K.

Compound	(1,5-PDA)BiI_5
Formula	$C_5H_{16}BiI_5N_2$
$D_{calc.}$/ g cm^{-3}	3.519
m/mm^{-1}	18.464
Formula Weight	947.68
Colour	dull dark black
Shape	rhombohedral-shaped
Size/mm^3	0.35×0.22×0.21
T/K	302.15(10)
Crystal System	orthorhombic
Flack Parameter	-0.020(4)
Hooft Parameter	-0.011(4)
Space Group	$P2_12_12_1$
a/Å	8.5824(4)
b/Å	14.7005(7)
c/Å	14.1760(7)
a/°	90
b/°	90
g/°	90
V/Å^3	1788.52(15)
Z	4
Z'	1
Wavelength/Å	0.71073
Radiation type	Mo K_a
Q_{min}/°	2.748
Q_{max}/°	30.884
Measured Refl's.	15677
Indep't Refl's	4599
Refl's I≥2 s(I)	3989
R_{int}	0.0529
Parameters	120
Restraints	0
Largest Peak	1.499
Deepest Hole	-2.589
GooF	1.051
wR_2 (all data)	0.0954
wR_2	0.0909
R_1 (all data)	0.0509
R_1	0.0411

Table S2. Bond Lengths in Å for (1,5-PDA)BiI_5.

Atom	Atom	Length/Å
Bi1	I1	3.2290(10)
Bi1	I1[1]	3.3144(10)
Bi1	I2	3.0817(12)
Bi1	I3	2.9792(10)
Bi1	I4	3.0460(11)
Bi1	I5	2.8928(11)

[1]1/2+x,1/2-y,1-z

Table S3. Bond Angles in ° for (1,5-PDA)BiI_5.

Atom	Atom	Atom	Angle/°
I1	Bi1	I1[1]	83.990(13)
I2	Bi1	I1[1]	85.72(3)
I2	Bi1	I1	87.44(3)
I3	Bi1	I1[1]	90.81(3)
I3	Bi1	I2	90.50(3)
I3	Bi1	I4	91.70(3)
I4	Bi1	I1[1]	86.07(3)
I4	Bi1	I1	89.64(3)
I5	Bi1	I1	87.39(3)
I5	Bi1	I2	97.36(4)
I5	Bi1	I3	97.90(3)
I5	Bi1	I4	90.44(3)

[1]1/2+x,1/2-y,1-z; [2]-1/2+x,1/2-y,1-z

Table S4. Summary of growth methods, trap density and carrier mobility of Bi-based materials.

Material	Growth method	Hole trap density (cm^{-3})	Carrier mobility ($cm^2 V^{-1} s^{-1}$)
$MA_3Bi_2I_9$ SC[1]	inverse temperature crystallization (ITC)	1.3×10^{10}	-
$(NH_4)_3Bi_2I_9$ SC[2]	slow solvent evaporation method	4.84×10^9	11
$(H_2MDAP)BiI_5$ SC[3]	top-seeded solution growth method	3.6×10^{11}	1.42
(3-AMP)BiI_5 SC[4]	temperature cooling technique	3.53×10^9	4.85×10^{-2}
$(BZA)_3BiI_6$ SC[4]	temperature cooling technique	4.25×10^{11}	6.16×10^{-3}
$FA_3Bi_2I_9$ SC[5]	secondary solution constant-temperature evaporation (SSCE) method	9.48×10^9	4
$Cs_3Bi_2Br_9$ SC[6]	solid slow cooling method	9.7×10^{10}	0.17
$Cs_3Bi_2I_9$ SC[7]	solution evaporation method	8.65×10^{10}	-
(1,5-PDA)BiI_5 SC （this work）	**liquid phase diffusion method**	**1.31×10^9**	**28.207**

References:

1. Tailor, N. K. *et al.* Influence of the A-site cation on hysteresis and ion migration in lead-free perovskite single crystals. *Phys. Rev. Mater.* **6**, 045401 (2022).
2. Zhuang, R. *et al.* Highly sensitive X-ray detector made of layered perovskite-like $(NH_4)_3Bi_2I_9$ single crystal with anisotropic response. *Nat. Photonics* **13**, 602–608 (2019).
3. Tao, K. *et al.* A Lead-Free Hybrid Iodide with Quantitative Response to X-ray Radiation. *Chem. Mater.* **31**, 5927–5932 (2019).
4. Yang, X., Huang, Y.-H., Wang, X.-D., Li, W.-G. & Kuang, D.-B. A-Site Diamine Cation

Anchoring Enables Efficient Charge Transfer and Suppressed Ion Migration in Bi-Based Hybrid Perovskite Single Crystals. *Angew. Chem. Int. Ed. 61*, e202204663 (**2022**).

5. Li, W. *et al.* Zero-Dimensional Lead-Free $FA_3Bi_2I_9$ Single Crystals for High-Performance X-ray Detection. *J. Phys. Chem. Lett.* **12**, 1778–1785 (2021).
6. Li, X. *et al.* Lead-free halide perovskite $Cs_3Bi_2Br_9$ single crystals for high-performance X-ray detection. *Sci. China Mater.* **64**, 1427–1436 (2021).
7. Li, L. *et al.* Centimeter-Sized Stable Zero-Dimensional $Cs_3Bi_2I_9$ Single Crystal for Mid-Infrared Lead-Free Perovskite Photodetector. *J. Phys. Chem. C* **126**, 3646–3652 (2022).